buildings

MDPI

Article

Experimental Test and Finite Element Analysis on a Concrete Box Girder of a Cable-Stayed Bridge with W-Shaped Prestressed Concrete Diagonal Braces

Xuhui He [1,2], Zhiyu Wang [1,2], Chao Li [1,2,*], Ce Gao [3], Yongfeng Liu [3], Changpeng Li [4] and Bin Liu [4]

[1] School of Civil Engineering, Central South University, Changsha 410075, China
[2] National Engineering Research Center for High-Speed Railway Construction Technology, Changsha 410075, China
[3] China Railway Engineering Design Consulting Group Co., Ltd., Beijing 100055, China
[4] Sichuan Longxuyi Railway Co., Ltd., Luzhou 646000, China
* Correspondence: lichaocsu@csu.edu.cn

Abstract: This paper presents an experimental study on the box girder of a low-tower cable-stayed railway bridge with a W-shaped section that consists of prestressed concrete diagonal braces. A 1:6 scale test model was designed and constructed for the experiment. The mechanical behavior of the test model was investigated under two loading conditions: a double-track train symmetrical load and a single-track train unsymmetrical load. The experimental results were validated against a finite element model. Furthermore, the torsional performance of the box girder section was analyzed and discussed.

Keywords: low tower cable-stayed bridge; W-shaped web box girder; mechanical; characteristics; torsional performance

Citation: He, X.; Wang, Z.; Li, C.; Gao, C.; Liu, Y.; Li, C.; Liu, B. Experimental Test and Finite Element Analysis on a Concrete Box Girder of a Cable-Stayed Bridge with W-Shaped Prestressed Concrete Diagonal Braces. *Buildings* **2024**, *14*, 506. https://doi.org/10.3390/buildings14020506

Academic Editor: Oldrich Sucharda

Received: 26 December 2023
Revised: 2 February 2024
Accepted: 9 February 2024
Published: 13 February 2024

1. Introduction

The single-plane cable-stayed bridge has a unique and visually appealing design. Its inclined pylons or towers, connected by diagonal cables, create a distinctive and elegant appearance. It also offers an efficient structural system that allows for longer spans compared to traditional beam bridges. The diagonal cables of a single-plane cable-stayed bridge provide strong support and distribute the load evenly, reducing the number of support piers required and allowing for wider navigation channels. The diagonal cables also improve the overall structural performance. They provide lateral stability, increase the bridge's ability to resist dynamic loads, such as winds and earthquakes, and minimize the bending moments on the bridge deck. It has been widely used in the field of highway engineering. For example, the Brotonne Bridge in France [1], completed in 1977, is a single-cable-plane cable-stayed bridge with a span combination of 143 + 320 + 143 m. The Sunshine Skyway Bridge [2] in the United States, completed in 1987, has a main span of 366 m and is also a single-cable-plane cable-stayed bridge (as shown in Figure 1). The bridge is 29 m wide and it has a beam height of 4.3 m and a cable spacing of 7.3 m. In the box-shaped cross-section, concrete bracings are arranged every 3.65 m. In China, many projects such as the Gan-Shen High-Speed Railway Jiantan Dongjiang Bridge (four-lane, central cable-stayed, main span 260 m), the Beijing Sixth Ring Road Fensha Railway Interchange Bridge (56 + 100 + 70 + 37 m), and the Baoding Lekai Street South Extension Project Cable-stayed Bridge across Baoding South Station (145 + 240 + 110 m) have adopted single-plane cable-stayed bridges in their designs.

(**a**) (**b**)

Figure 1. (**a**) The Sunshine Skyway bridge; (**b**) LeKai South Extension bridge.

When using a single-cable-plane design, the torsional resistance of the cable to the girder is relatively weak (and can even be ignored), so the main girder needs to have a box-shaped cross-section with high torsional stiffness [3]. The commonly used cross-sectional forms include single-box multi-cell sections and W-shaped web box girder sections. For the W-shaped web box girder section, the cables are anchored in the middle of the cross-section, and the web plates, top, and bottom plates form a truss system. In this design, cables are anchored in the middle of the cross-section, and the various components of the box girder, including the web plates, top plate, and bottom plate, form a truss system. In the truss-like system, the two diagonal braces in the truss system are in tension, while the two outer vertical web plates and the bottom plate of the box girder are in compression. By incorporating the truss system within the box girder, the forces can be transferred more efficiently, and it eliminates the need for traditional cross beams or transverse beam structures. This makes it convenient for formwork construction, steel reinforcement fixing, and formwork removal during the cantilever pouring construction process, thus greatly increasing the construction speed. Such innovations in bridge design are aimed at optimizing material usage, reducing weight, and enhancing the overall structural efficiency of the bridge.

Based on past engineering experience, the construction of the traditional W-shaped diagonal web box girder's top plate, diagonal web plate supports, and formwork installation is somewhat inconvenient [4]. The formworks of the top plate need to be supported by the web plate formwork (as shown in Figure 2). When there are changes in the height of the girder, the height and diagonal angle of the W-shaped web also change, forming a spatial curve surface. This leads to complex formwork processing and installation, making the on-site construction challenging. Therefore, this type of cross-sectional design still requires further optimization and improvement. Currently, there are few construction cases for single-cable-plane cable-stayed bridges in the railway sector. In this study, a railway single-cable-plane low tower cable-stayed bridge is used as a basis to propose a W-shaped cross-sectional design with longitudinally spaced concrete diagonal braces. By using longitudinally spaced diagonal braces instead of a continuous diagonal web, the difficulties of formwork preparation caused by the variation in beam heights can be solved. Moreover, it also facilitates the construction of the top plate formwork. The diagonal braces are equipped with pre-stressed steel bars to effectively resist the vertical forces from the cables, and the pre-stressing force in the diagonal braces can effectively prevent significant deformations in the top plate. Currently, there are no completed cases of single-cable-plane railway cable-stayed bridges with a span of 300 m in China and the proposed W-shaped cross-section with diagonal braces is novel. Therefore, it is necessary to conduct research on the mechanical performance of the girder.

Figure 2. W-shape diagonal web section construction.

Many researchers have conducted relevant research on the stress characteristics of box girders, including experimental studies and theoretical analyses [5–9]. Kim et al. [10] conducted three-dimensional finite element analyses and determined the ultimate strength of composite box girders in bending and torsion. Chidolue et al. [11] conducted a comparative analysis of the torsional distortion effects of conventional single-cell box girders with diagonal bracings and three-cell box girders with two additional diagonal bracings. The results showed that the distortion deformation of the three-cell box girders with full diagonal bracings can be reduced by 168%. Li et al. [12] carried out analytical and numerical studies on composite box girders with corrugated steel webs. Mo et al. [13] conducted an analytical study on the torsional performance of a hybrid concrete box girder.

Since this study adopts the W-shaped cross-section form of pre-stressed concrete diagonal braces arranged longitudinally at intervals, the performance of the box girder could be different from that of traditional box girders with a continuous web along the longitudinal direction of the bridge. Therefore, it is necessary to conduct a systematic study of this new structural form. In this paper, a scaled-down test model with a scale of 1:6 was constructed and tested. Based on the test, a finite element model was established and the test results were verified and analyzed. The research results can accumulate engineering experience for the further application of such designs in railway or highway construction projects.

2. Experimental Research

2.1. Project Overview

As shown in Figure 3, the bridge in this project is a three-span low tower cable-stayed railway bridge with a single-cable plane and two towers. The top plate of the main girder is 15.8 m wide, the bottom plate width is 11.7 m, and the bridge tower is 5.5 m high. The height of the girder transitions from 8 m at the mid-span to 14 m at the central support point. Specifically, the height of the girder beneath the central support point varies in a parabolic manner over a length of 71 m on each side, while the rest of the girder maintains a constant height of 8 m. The cross-sectional form is characterized by the use of a W-shaped profile with pre-stressed concrete diagonal braces arranged longitudinally at intervals, and the outer web plate is vertical.

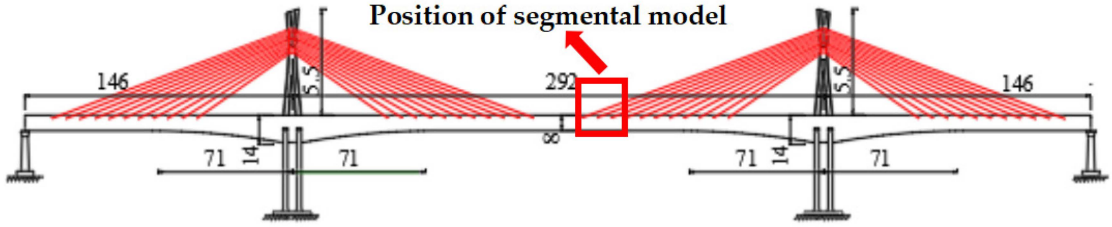

Figure 3. Elevation layout of the railway bridge (unit: m).

2.2. Test Model

The experimental model was designed according to similarity criteria. Taking into consideration the capabilities of the testing facility, the scale ratio of the model was set at 1:6. As shown in Figure 4, this model consists of the main girder, diagonal cables, and a reaction frame. Based on the scale ratio, the dimensions of the scaled model are 7.75 m in length, 2.63 m in width, and 1.33 m in height. The top plate of the test section is 2.63 m wide and 67 mm thick, while the bottom plate is 1.95 m wide and 67 mm thick. The web plate is 83 mm thick and has a height of 1.2 m. Additional cross-sectional dimensions are provided in Figures 5 and 6.

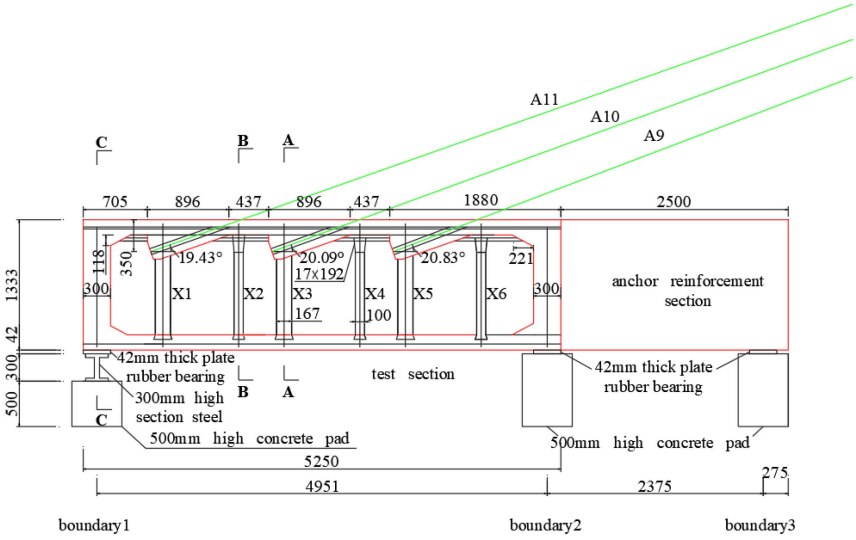

Figure 4. Overall layout of the test model (unit: mm).

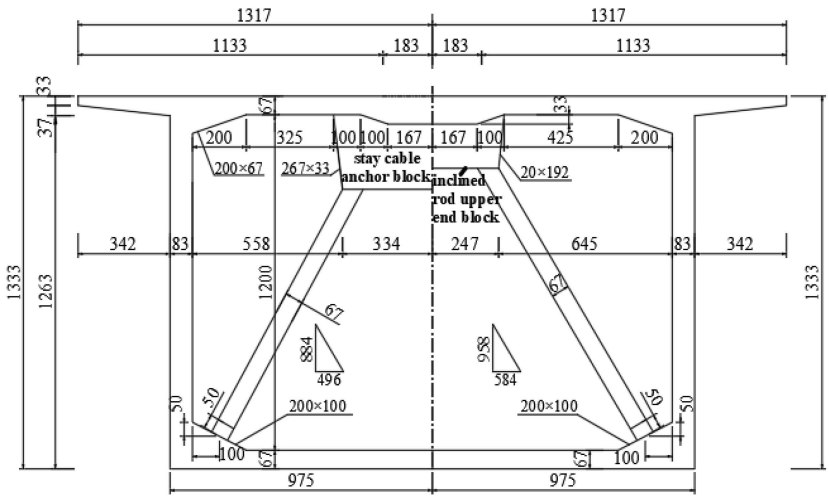

Figure 5. A-A section (**left**); B-B section (**right**) (unit: mm).

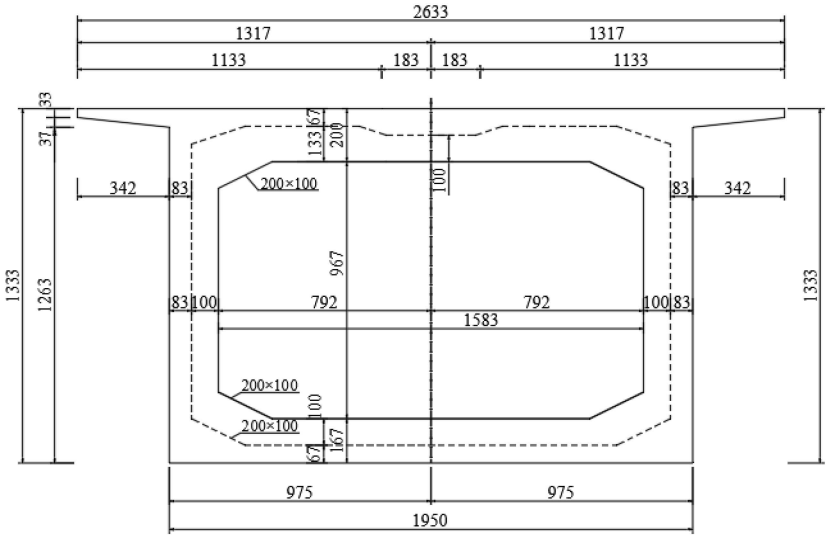

Figure 6. Section of end thickening and anchor reinforcement (C-C section, unit: mm).

For the steel reinforcement, the pre-stressing tendons in the model include a total of nine transverse pre-stressing tendons in the top slab, six pairs of longitudinal pre-stressing tendons running along the full length of the top slab, and an additional three pairs of external tendons symmetrically arranged along the central axis of the top slab. There are also nine longitudinal pre-stressing tendons running along the full length of the bottom slab. The layout of pre-stressing tendons is shown in Figures 7 and 8. Each diagonal bar has one pre-stressing tendon, arranged at the center position of the diagonal braces, thus a total number of 12 pre-stressing tendons are adopted in the diagonal braces. In addition, to simulate the effect of diagonal cables, three diagonal cables (A11, A10, A9) and three vertical tension cables (A11′, A10′, A9′) are anchored in the anchoring blocks. The high- strength strands with a diameter of 15.2 mm are used for the pre-stressing tendons, vertical cables, and diagonal cables. Ordinary steel reinforcement includes longitudinal bars, stirrups, and transverse ordinary steel reinforcement, all of which use HRB400 steel bars with a diameter of 6 mm.

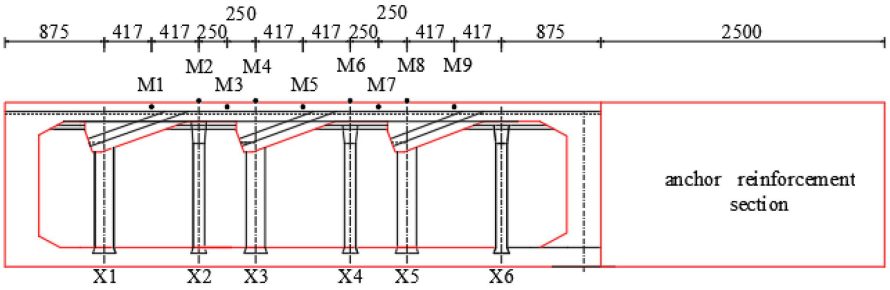

Figure 7. Longitudinal bridge arrangement of transverse pre-stressed reinforcements on the top plate (unit: mm).

2.3. Test Program

2.3.1. Test Setup

Figure 9 shows the test setup of the specimen. In general, it consists of vertical supports for the beam, a steel tower that simulates the tower of the prototype bridge, and a steel frame that serves as the anchorage frame of the cables and also the horizontal support for the beam. As shown in Figure 9, the box girder was supported on three boundaries: boundary 1, boundary 2, and boundary 3. Boundary 1 employed steel beams with hinge supports at the mid-span to release the torsional degrees of freedom of the girder end. Boundary 2 used rubber plate-type supports, and boundary 3 employed rubber plate-type

supports along with a steel beam to anchor the girder ends to the strong floor of the lab. The end of the girder at boundary 3 was attached to the steel tower, which restrained the lateral deformation of the whole beam. To apply the vertical loading, another three vertical loading frames were constructed. The frames were installed at the load points illustrated in Figure 9 (in the longitudinal locations of the girder). The schematic drawing of the loading frames and the horizontal locations of the load points are shown in Figure 10.

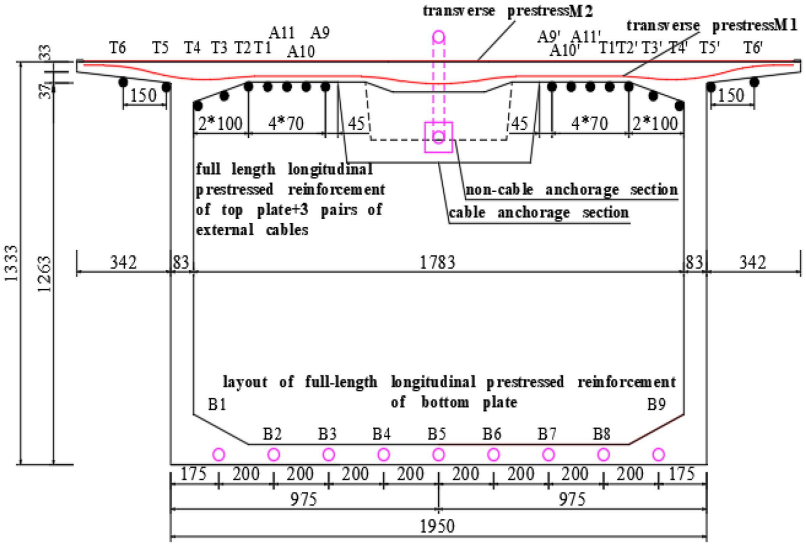

Figure 8. Cross-sectional layout of the longitudinal pre-stressed reinforcement for the full length of the top and bottom plates (unit: mm).

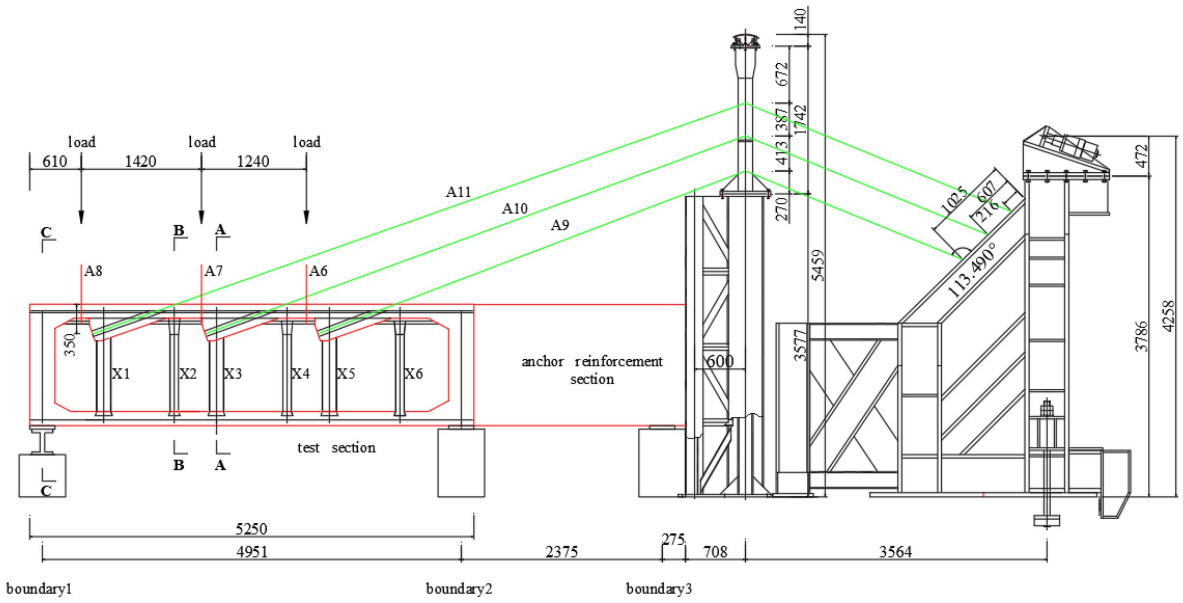

Figure 9. Longitudinal bridge layout of loading points, vertical stay cables, stay cables, and the reaction frame (unit: mm).

2.3.2. Loading Protocol

During the test, three categories of loadings were applied to the specimen, including the added dead load, pre-stressing forces in the tendon, and the applied service load. The dead load was applied by adding steel blocks in the box girder and above the top surface of the girder. For the pre-stressing forces, a hydraulic jack was used to apply the post-tensioned force to the aimed values. For the service load, six loading points were

installed with hydraulic jacks. The load protocol was determined based on the standard Code for Design on Railway Bridge and Culvert: TB10002-2017 [14] and it was scaled following the scale factor and the similitude law. The load was static since the aim of the study was to investigate the static performance of the girder. An initial force of 28.2 kN was applied to the loading points, acting as the supplementary of the dead load. Then, two loading cases were conducted to mimic the double-track train symmetrical load and single-track train unsymmetrical load conditions. For the double-track train symmetrical load condition, the loads were applied simultaneously to all six hydraulic jacks and the forces at the loading points were monitored by load cells. The forces in the jacks increased gradually from 34.2 kN, 40.2 kN, 43.2 kN, 46.2 kN, 49.2 kN, 52.2 kN, and 55.2 kN to the maximum considered force of 57 kN. When the test was finished, the six loading points were all unloaded to 28.2 kN. After the unloading was completed, eccentric loads were applied in eight stages, that is, the loads of 34.2 kN, 40.2 kN, 43.2 kN, 46.2 kN, 49.2 kN, 52.2 kN, 55.2 kN, and 57 kN were applied sequentially at three loading points on one side only.

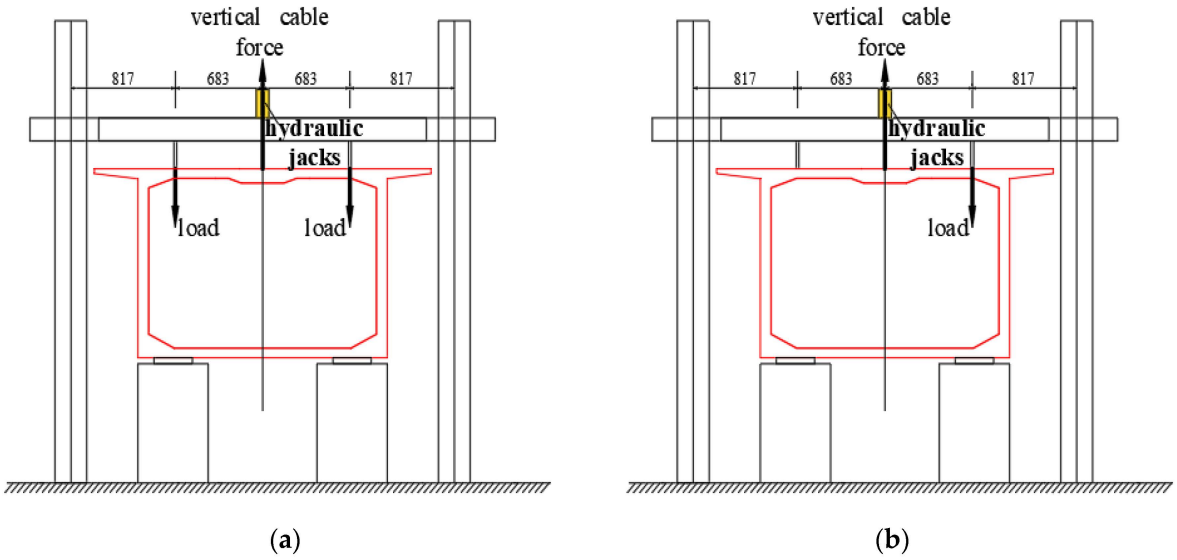

Figure 10. Schematic diagram of loading points under working conditions: cross-sectional view (**a**) symmetrical load; (**b**) unsymmetrical load (unit: mm).

2.3.3. Instrument Layout

At the completion of each stage of loading, the deflection and strain data of the model were recorded. The deflections of the specimen were recorded by JMDL-3150AT displacement sensors installed at the bottom of the box girder and the arrangement of the sensors is shown in Figure 11. During the test, vertical displacements of the girder were measured and recorded under different loading levels. In addition, the strain gauges were attached to the steel bars in the diagonal post-tensioned braces along the longitudinal direction of the braces. Since the braces of the X3 section were critical for the analysis, the strains of the steel bars in the braces of this section were measured. The layout of the strain gauges is shown in Figure 12. As shown, 3A-1 and 3B-1 represent the strain gauges installed on the exterior side of the steel bars in the left- and right-side braces near the bottom plate, respectively. Similarly, 3A-8 and 3B-8 represent the strain gauges installed on the exterior side of the steel bars in the left- and right-side braces near the top plate, respectively. All the strain gauges were connected to a DH3816 data acquisition system. The strains at different levels of loading were recorded during the test. The final setup of the test model prior to the test is shown in Figure 13.

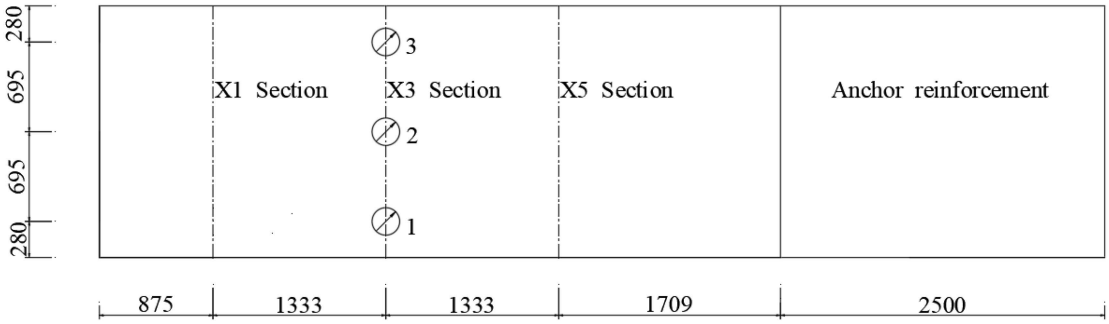

Figure 11. Plane layout of displacement sensors (unit: mm).

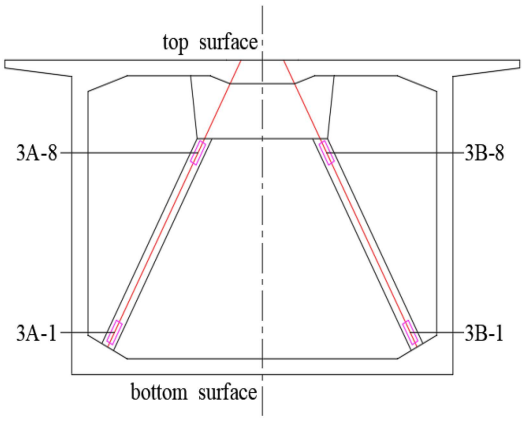

Figure 12. Arrangement of strain gauges in the X3 section.

Figure 13. Final setup of the test.

3. Test Results and Discussions

3.1. Deflection of the Girder

From the test results (Table 1 and Figure 14), it can be seen that under the double-track train symmetrical load, the deflection of the mid-span increased linearly with the load, which demonstrated that the girder was in a linear-elastic state. The measured deflection values of the three measuring points arranged along the mid-span are similar under the symmetrical loads. From the test results (Table 2 and Figure 15), it can be seen that under the unsymmetrical loads, the deflection of the mid-span also increases linearly with the load. However, due to the unsymmetrical loads, the measured deflection values of the three points are different. It is evident that the unsymmetrical load resulted in the torsional deformation of the girder.

Table 1. Deflection of the mid-span under a symmetrical load (unit: mm).

Load Value	34.2 kN	40.2 kN	43.2 kN	46.2 kN	49.2 kN	52.2 kN	55.2 kN	57 kN
Point 1	−0.06	−0.12	−0.15	−0.18	−0.2	−0.23	−0.26	−0.28
Point 2	−0.06	−0.1	−0.13	−0.15	−0.18	−0.2	−0.23	−0.25
Point 3	−0.06	−0.11	−0.13	−0.16	−0.18	−0.2	−0.23	−0.25

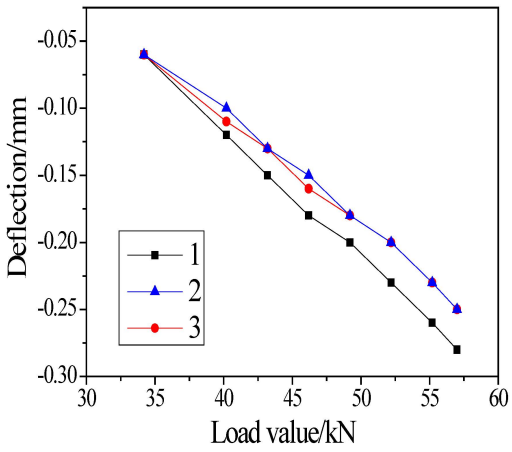

Figure 14. Deflection of the specimen under the symmetrical loads.

Table 2. Deflection of the specimen under a single-track unsymmetrical load (unit: mm).

Load Value	34.2 kN	40.2 kN	43.2 kN	46.2 kN	49.2 kN	52.2 kN	55.2 kN	57 kN
Point 1	−0.03	−0.07	−0.09	−0.11	−0.14	−0.15	−0.17	−0.18
Point 2	−0.01	−0.03	−0.03	−0.05	−0.06	−0.07	−0.08	−0.09
Point 3	−0.01	−0.03	−0.04	−0.05	−0.05	−0.06	−0.07	−0.08

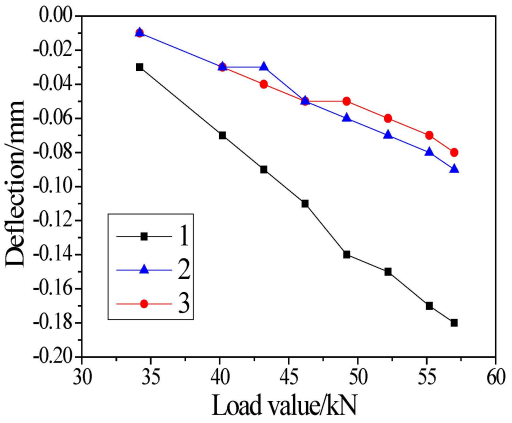

Figure 15. Deflection of the specimen under the unsymmetrical loads.

3.2. Strain Results

The strains of measuring points under graded symmetrical loads are shown in Table 3 and Figure 16. From the test results, it can be seen that the steel bars in the X3 diagonal braces were all under tension. The largest strain was around 13 με, which is much smaller than the yield strain of steel (i.e., about 2000), demonstrating that the steel bar did not experience any plastic deformation during the test. The strains of measuring points under graded unsymmetrical loads are shown in Table 4 and Figure 17. From the test results, the strain distribution of the steel bars in the diagonal brace is also unsymmetrical due to the applied unsymmetrical loads. The steel bars had tensile and compressive strains depending on their locations. Among them, measuring point 3A-8 at the top of the X3

diagonal brace steel bar on the side without load has the largest tensile strain value of 10 με. Measuring point 3B-1 at the bottom end of the X3 inclined rod steel bar on the side with the applied load has the largest compressive strain value of 17 με.

Table 3. Strain value of measuring points under graded symmetrical loads (unit: με).

Measuring Points	34.2 kN	40.2 kN	43.2 kN	46.2 kN	49.2 kN	52.2 kN	55.2 kN	57 kN
3A-1	2	3	3	4	5	6	7	8
3A-8	2	4	5	6	7	8	9	10
3B-1	2	3	4	4	5	6	7	8
3B-8	2	3	4	5	5	6	7	8

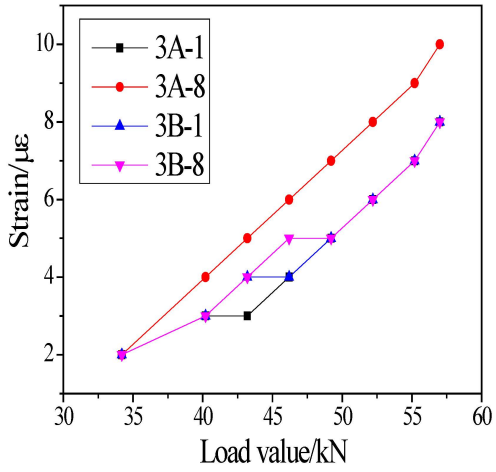

Figure 16. Strain of measuring points under graded symmetrical loads.

Table 4. Strains of measuring points under graded unsymmetrical loads (unit: με).

Measuring Points	34.2 kN	40.2 kN	43.2 kN	46.2 kN	49.2 kN	52.2 kN	55.2 kN	57 kN
3A-1	2	3	4	4	5	6	7	8
3A-8	2	4	5	6	7	8	9	10
3B-1	−3	−5	−6	−9	−10	−14	−16	−17
3B-8	−2	−4	−6	−7	−7	−8	−8	−9

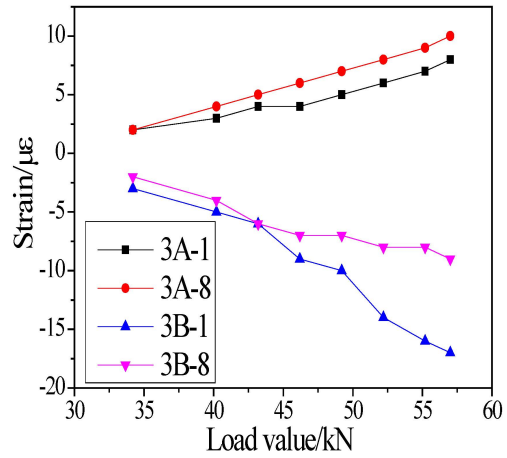

Figure 17. Strain value of measuring points under graded unsymmetrical loads.

4. Finite Element Analysis

4.1. Numerical Model

In this section, ABAQUS was used to simulate the behavior of the specimen [15]. The concrete, pre-stressed strands, and pre-stressed cables were simulated by solid-element C3D8R. The steel bars were modelled by the three-dimensional two-node truss element T3D2 in ABAQUS. The C3D8R element is an eight-node linear brick element with reduced integration. This type of element is often used for three-dimensional structural analysis. Each node of the C3D8R element has three translational degrees of freedom (DOFs), representing displacements in the X, Y, and Z directions. Therefore, each C3D8R element has 24 DOFs. The T3D2 element is a three-dimensional truss element with six DOFs. In terms of connection types between the components, this numerical model has three types of connections, namely tie, embedded, and coupling. The steel bars were embedded in the surrounding concrete. For the boundary condition, the bottom surfaces of the rubber bearings were fully constrained, while the top surfaces of the rubber bearings were in contact with the concrete beam. The middle point of the steel beam was constrained in the X, Y, and Z directions, but the rotational degrees of freedom were released to simulate the hinge installed at this point. For the symmetrical loading condition, two corners of the bottom plate of the beam at the left-side end in Figure 18a were constrained in the vertical direction. In contrast, for the unsymmetric loading condition, these constraints were released. Regarding the element sizes of the FE model, the mesh convergence test was conducted when developing the numerical models. A mesh size of 0.02 m was determined for the region between braces X2–X3, while the element size of the rest of the model was 0.1 m. These values were chosen to obtain accurate results with a reasonable calculating time. The total model is divided into 817,713 elements. To apply the loadings at the designed loading points, reference points are set and coupled together with the concrete surface and the loads were then applied to the reference points.

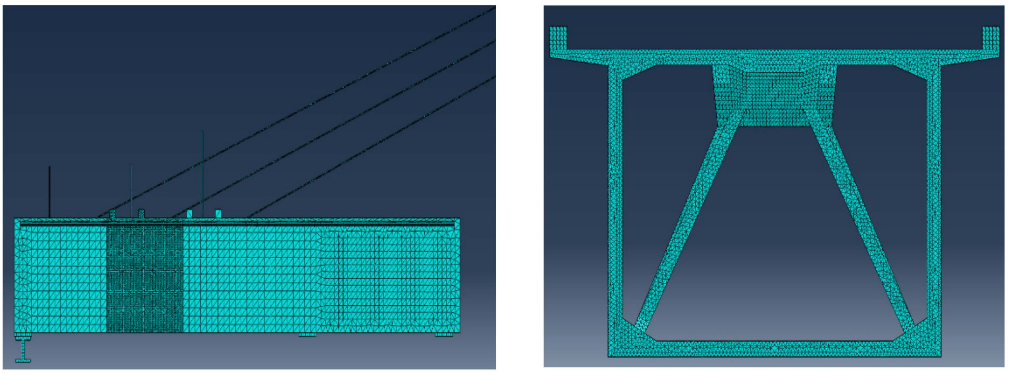

(**a**) (**b**)

Figure 18. Finite element model: (**a**) side view; (**b**) cross-section view.

4.2. Analysis Results

4.2.1. Comparison between Modelling and Test Results of the Deflection

Figure 19 shows the comparison between the modelling and test results of the three deflection measuring points in the mid-span under graded symmetrical loads. It can be seen from the Figure that the theoretical results are consistent with the test results, and the relative errors are mostly smaller than 16%. Under the load of 57 kN, the maximum test result of the deflection measuring points in the mid-span is 0.28 mm and the corresponding modelling result is 0.236 mm, which is quite close to the test result. Therefore, it can be seen that the developed finite element model is accurate in predicting the deformation of the tested girder. Figure 20 shows the comparison between the test and the theoretical results of the three deflection measuring points in the mid-span under graded unsymmetrical loads. It can be seen from the figure that under the graded unsymmetrical loads, the theoretical results are also consistent with the test results. Under the unsymmetrical load of 57 kN, the

maximum modelling and test results of the deflection measuring points in the mid-span are 0.149 mm and 0.18 mm, respectively.

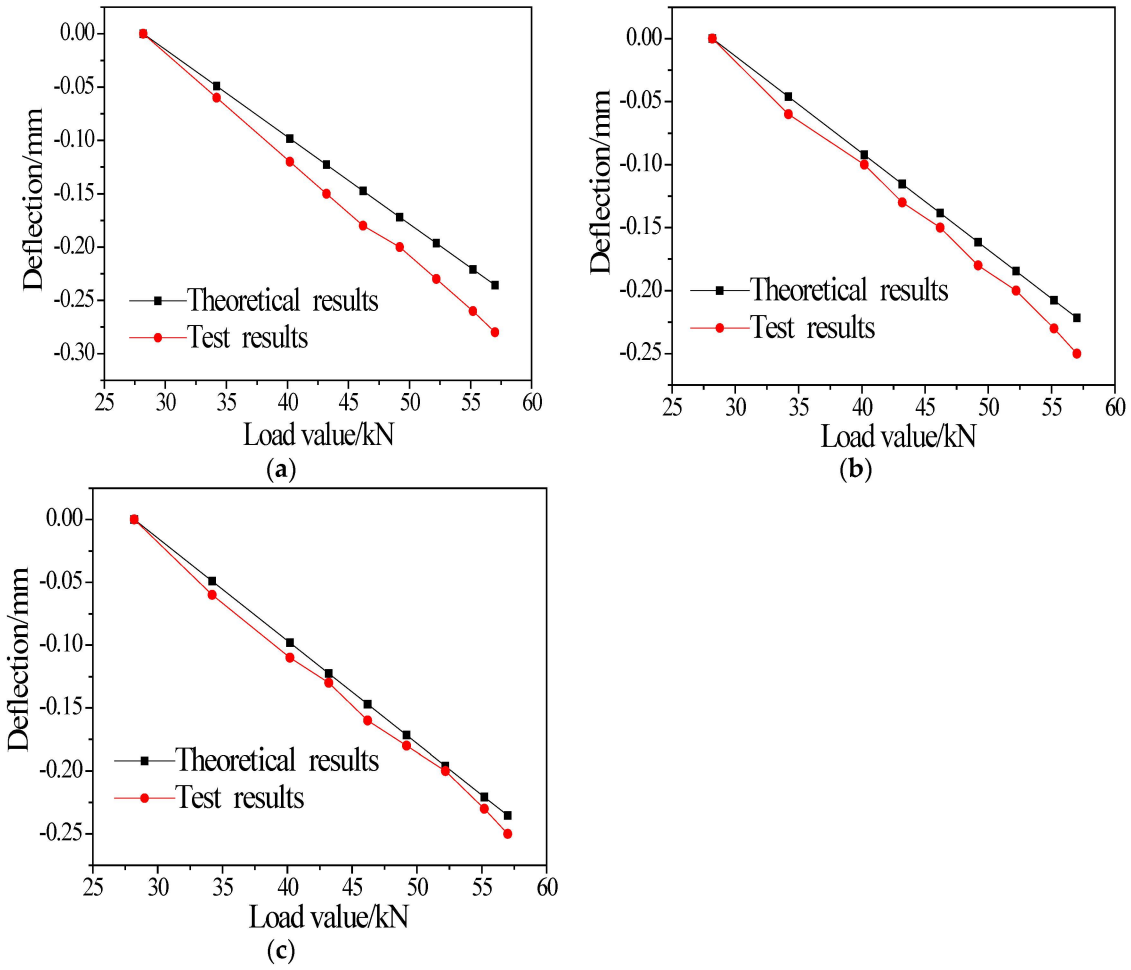

Figure 19. Comparison between theoretical and test results of deflection under graded symmetrical loads (**a**) point 1; (**b**) point 2; (**c**) point 3.

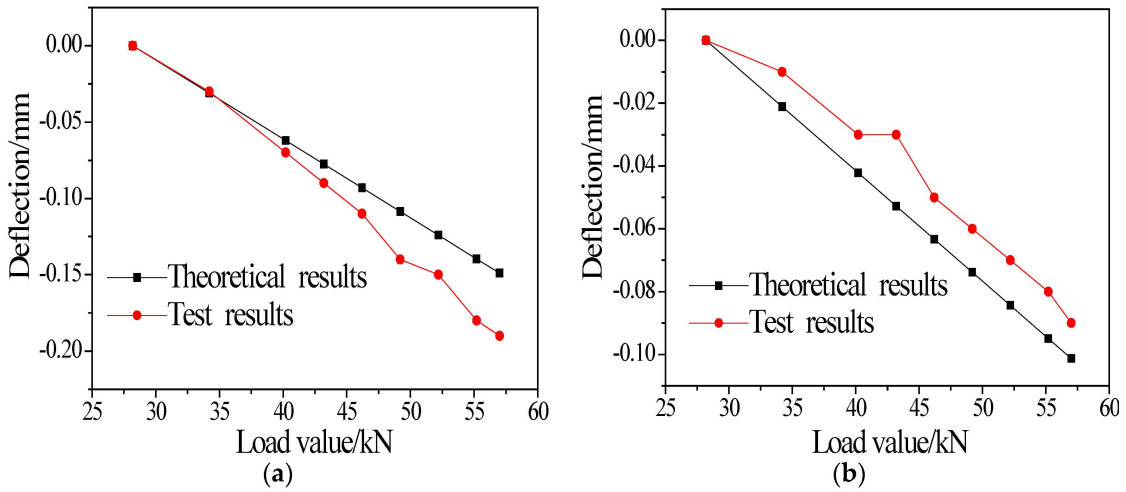

Figure 20. *Cont.*

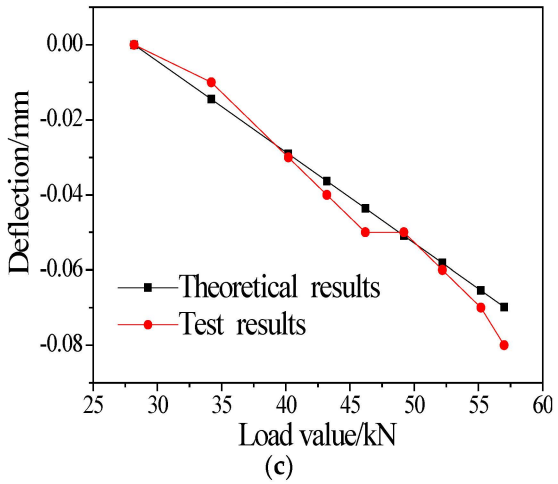

Figure 20. Comparison between theoretical and test results of deflection under graded unsymmetrical loads (unit: mm): (**a**) point 1; (**b**) point 2; (**c**) point 3.

4.2.2. Comparison of the Strains

Figure 21 shows the comparison between the modelling and test results of strains under graded symmetrical loads. For example, under the symmetrical load of 57 kN, the maximum strain of the modelling result was 8.86 με, and the corresponding test result was 10 με, resulting in a relative error of 11.4%. The overall relative error was slightly less than 20%. Figure 22 shows the comparison between the modelling and test results of strain under graded unsymmetrical loads. Under the 57 kN load, the modelling maximum tensile strain was 9.95 με and the corresponding test result was 10 με, which demonstrated that the difference was relatively small. The modelling and test results of the maximum compressive strains were 15.07 με and 17 με, respectively, and the predicting error was only 11.35%.

4.3. Torsional Performance of the W-Shaped Web Box Girder

When the girder is subjected to unsymmetrical loads, its torsional effect is normally obvious. The torsion angle under unsymmetrical loads is used for the analysis in the following section, and the calculation method of the torsion angle is shown in Figure 23.

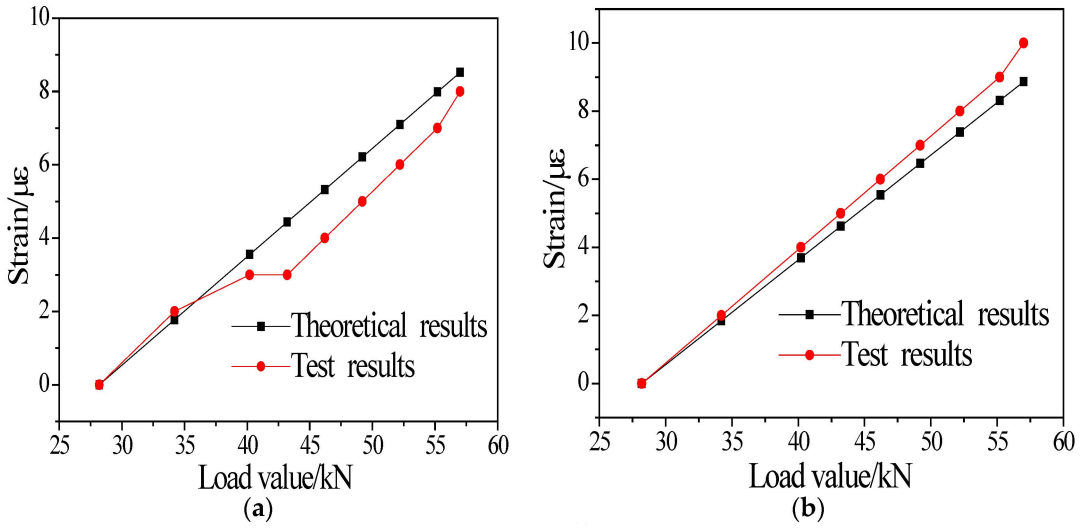

Figure 21. *Cont.*

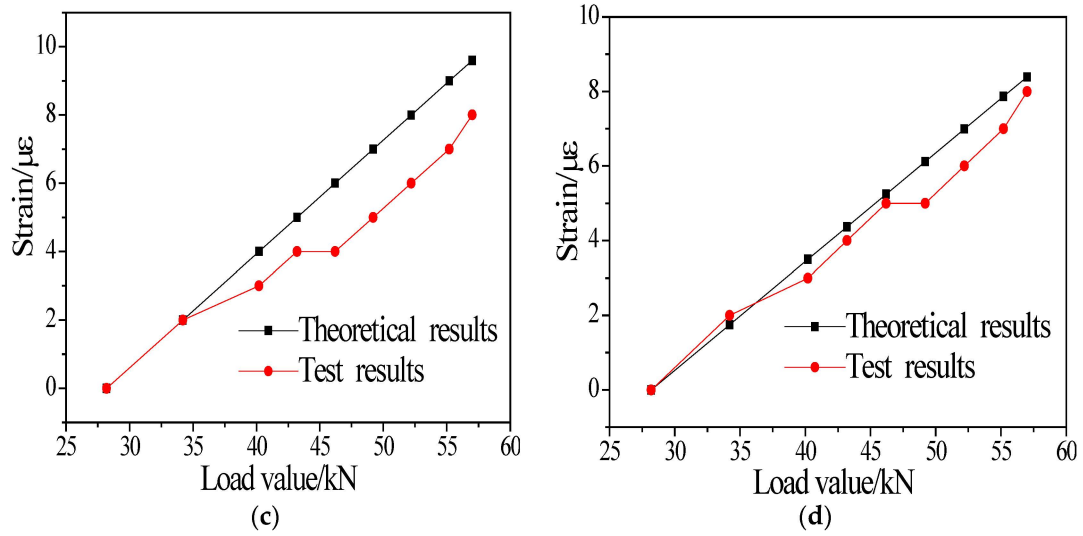

Figure 21. Comparison between theoretical and test results of strain under graded symmetrical loads: (**a**) 3A-1; (**b**) 3A-8; (**c**) 3B-1; (**d**) 3B-8.

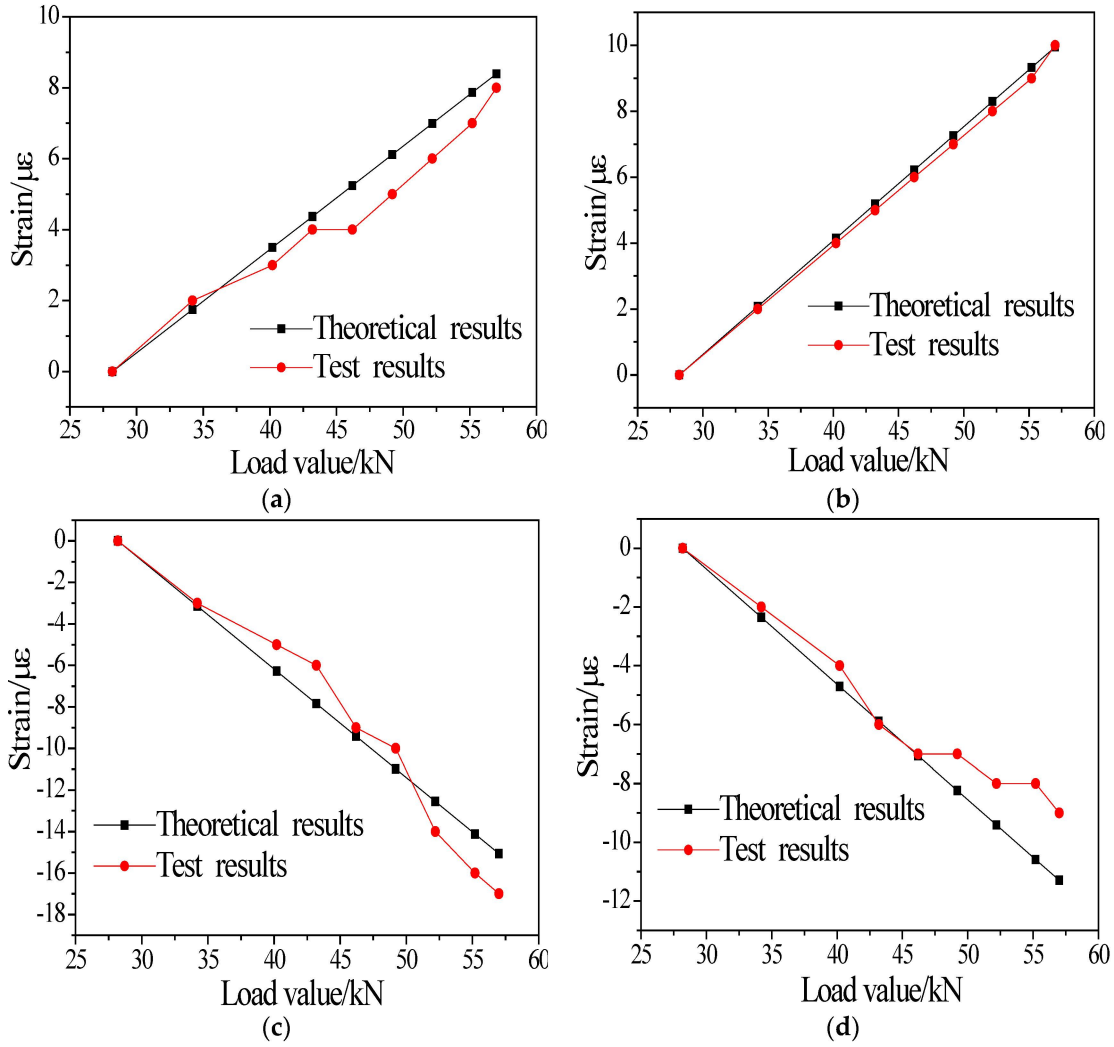

Figure 22. Comparison between theoretical and test results of strain under graded unsymmetrical loads: (**a**) 3A-1; (**b**) 3A-8; (**c**) 3B-1; (**d**) 3B-8.

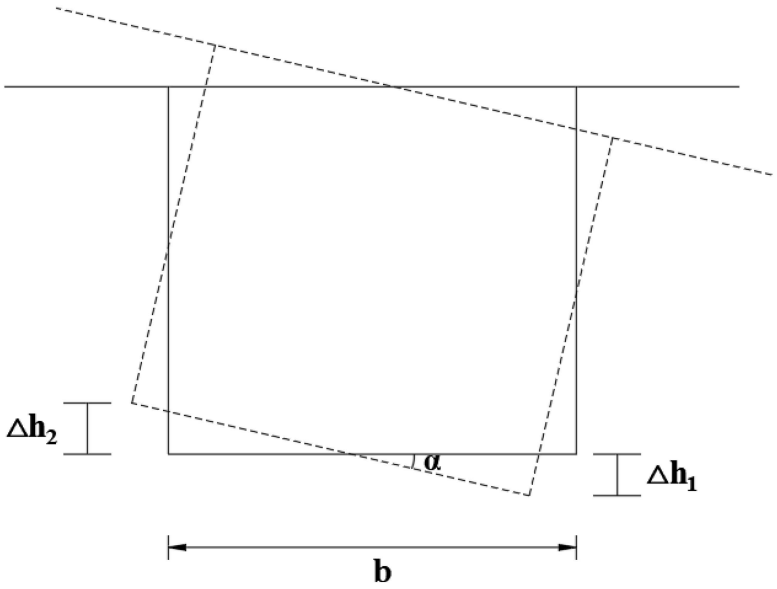

Figure 23. Schematic diagram of calculation method of the torsion angle.

The torsion angle is:

$$\alpha = \frac{\Delta h_1 + \Delta h_2}{b} \quad (1)$$

In the formula, α is the torsional angle, b is the width of the bottom plate, and Δh_1 and Δh_2 are the displacements. Figure 24 depicts the variation of the torsional angle with respect to the longitudinal coordinate of the girder. In general, the torsional angle increased with increases in loading levels. Along the longitudinal direction of the girder, the torsional angle had the maximum value at the free end, which is attributed to the fact that the freedom of rotation along the girder's longitudinal axis was released at the free end by using the single-point-supported cross beam. Under the unsymmetrical load of 57 kN, the maximum torsion angle is 0.006°. The maximum torsion angle is less than the value that was reported in a reference (0.019°), in which the torsional angle of a simple supported railway box girder was investigated [16]. Therefore, it demonstrated that the torsional stiffness of the girder tested in this study is sufficient to resist unsymmetrical loading and that the torsional deformation is not obvious. In other words, the diagonal braces used in the design of the box girder are effective in improving the overall performance of the girder under unsymmetrical loading.

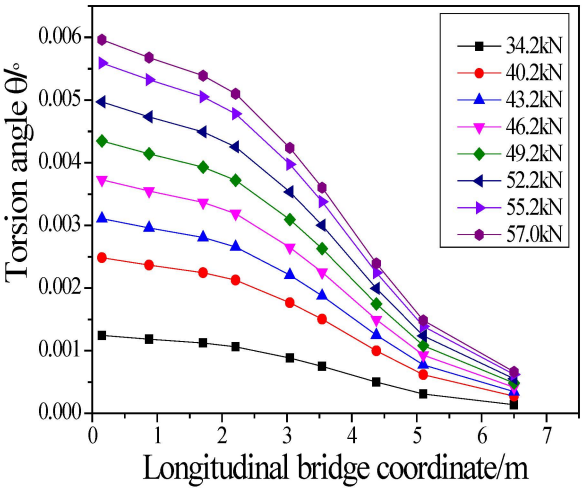

Figure 24. Torsion angle vs. longitudinal bridge coordinate change diagram.

5. Conclusions

In this paper, experimental study and finite element simulation were conducted to investigate the performance of a W-shaped section that consists of pre-stressed concrete diagonal braces. Based on the test and numerical results, the following conclusions are drawn:

(1) It can be seen from the test that under the applied loads during the test, the deflection and strain increments were linear as the load increased, indicating that the girder was in a linear elastic state in the test. No visible concrete cracks were observed. Under the unsymmetrical loads, the measured deflection values of the three points are different. It is evident that the unsymmetrical loads resulted in the torsional deformation of the girder.

(2) A detailed numerical model was developed in the software ABAQUS 6.13, and the relative error between model results and test results is less than 16%. Therefore, the deflection and strain of the box girder model could be calculated accurately, indicating that the numerical model developed in this study was accurate.

(3) The torsional performance of the box girder was also investigated based on the developed numerical model. According to the results, the maximum torsion angle (0.006°) was less than the value reported in a reference (0.019°), demonstrating that the torsional stiffness of the girder tested in this study was sufficient to resist the unsymmetrical loading and that torsional deformation was not obvious.

Author Contributions: Conceptualization, X.H.; Data curation, Z.W. and C.L. (Changpeng Li); Investigation, C.G. and B.L.; Methodology, C.G. and C.L. (Changpeng Li); Resources, Y.L.; Software, C.L. (Chao Li), Y.L. and B.L.; Supervision, X.H. and C.L. (Changpeng Li); Writing—original draft, Z.W.; Writing—review & editing, X.H. and C.L. (Changpeng Li). All authors have read and agreed to the published version of the manuscript.

Funding: This work is financially supported by Science and Technology Development Project of China Railway Engineering Design Consulting Group Co., Ltd.: Design Research of Single Plane Cable-Stayed Bridge for Passenger and Freight Collinear Railway (Research 2021-25); Science and Technology Research and Development Plan of China Railway Corporation: Research and Application of New Bridge Structures and High-Performance Materials (2021-Special Project-02); Sichuan Shudao Railway Investment Group Co., Ltd.; Science and Technology Innovation Project: Research on key technologies of railway W-shaped cross-section concrete box girder single cable plane long-span short tower cable-stayed bridge (SDTL2023ZD001).

Data Availability Statement: The data presented in this study are available on request from the corresponding author.

Conflicts of Interest: Authors Ce Gao and Yongfeng Liu were employed by the company "China Railway Engineering Design Consulting Group Co., Ltd.", And Authors Changpeng Li and Bin Liu were employed by the company "Sichuan Longxuyi Railway Co., Ltd.", The remaining authors declare that the research was conducted in the absence of any commercial or financial relationships that could be construed as a potential conflict of interest.

References

1. Lenglet, C. Brotonne Bridge Longest Prestressed Concrete Cable Stayed Bridge. In *Cable-Stayed Bridges, Structural Engineering Series*; Bridge Division, Office of Engineering, Federal Highway Administration: Washington, DC, USA, 1978.
2. Svensson, H.S.; Christopher, B.G.; Saul, R. Design of a cable-stayed steel composite bridge. *J. Struct. Eng.* **1986**, *112*, 489–504. [CrossRef]
3. Hao, Q.; Jufeng, S.; Pingming, H. Study on dynamic characteristics and seismic response of the extradosed cable-stayed bridge with single pylon and single cable plane. *J. Civ. Struct. Health Monit.* **2017**, *7*, 589–599. [CrossRef]
4. Huang, W.; Pei, M.; Liu, X.; Wei, Y. Engineering, C. Design and construction of super-long span bridges in China: Review and future perspectives. *Front. Struct. Civ. Eng.* **2020**, *14*, 803–838. [CrossRef]
5. Soto, A.G.; Caldentey, A.P.; Peiretti, H.C.; Benítez, J.C. Experimental behaviour of steel-concrete composite box girders subject bending, shear and torsion. *Eng. Struct.* **2020**, *206*, 110169. [CrossRef]
6. Arici, M.; Granata, M.F.; Longo, G. Symplectic analysis of thin-walled curved box girders with torsion, distortion and shear lag warping effects. *Thin Wall. Struct.* **2022**, *175*, 109244. [CrossRef]

7. He, X.; Sheng, X.; Scanlon, A.; Linzell, D.; Yu, X. Skewed concrete box girder bridge static and dynamic testing and analysis. *Eng. Struct.* **2012**, *39*, 38–49. [CrossRef]
8. Zhu, M.; Yan, Z.; Chen, L.; Lu, Z.; Chen, Y.F. Experimental study on composite mechanical properties of a double-deck prestressed concrete box girder. *Adv. Struct. Eng.* **2019**, *22*, 2545–2556. [CrossRef]
9. Campo-Rumoroso, I.; Ramos-Gutiérrez, Ó.R.; Cambronero-Barrientos, F. Distortion analysis of horizontally curved trapezoidal box girder bridges. *Eng. Struct.* **2023**, *282*, 115798. [CrossRef]
10. Kim, K.; Yoo, C.H. Ultimate strength interaction of bending and torsion of steel/concrete composite trapezoidal box girders in positive bending. *Adv. Struct. Eng.* **2006**, *9*, 707–718. [CrossRef]
11. Chidolue, C.; Amadou, A.; Ezeagu, C. Torsional-distortional performance of multi-cell trapezoidal box girder with all inclined web members. *Int. J. Eng. Res.* **2015**, *5*, 45–51.
12. Li, L.; Zhou, C.; Wang, L. Distortion analysis of non-prismatic composite box girders with corrugated steel webs. *J. Constr. Steel Res.* **2018**, *147*, 74–86. [CrossRef]
13. Mo, Y.; Fan, Y.-L. Torsional design of hybrid concrete box girders. *J. Bridge Eng.* **2006**, *11*, 329–339. [CrossRef]
14. National Railway Administration of the People's Republic of China. *Code for Design on Railway Bridge and Culvert*; China Railway Publishing House: Beijing, China, 2017.
15. Simulia, D.S. *Abaqus 6.12 Documentation*; Dassault Systèmes Simulia Corp.: Providence, RI, USA, 2012.
16. Li, Q.; Hu, S.; Shi, L.; Su, Y. Analysis of Torsion Deformation Performance of Railway Simply Supported Box Girder. *Railw. Eng.* **2021**, *61*, 1–5. (In Chinese)